LA-6459-MS
Informal Report



UC-20 and UC-34c
Reporting Date: July 1976
Issued: August 1976

# Neutron Background Spectra and Signal-to-Background Ratio for Neutron Production Between 10 and 14 MeV by the Reactions $^{3}H(p,n)^{3}He$, $^{1}H(t,n)^{3}He$, and $^{2}H(d,n)^{3}He$

by

Manfred Drosg*
George F. Auchampaugh
Flavio Gurule

*Visiting Staff Member. University of Vienna, Strudlhofg. 4, A-1090 Wien, Austria.



los alamos
scientific laboratory
of the University of California
LOS ALAMOS, NEW MEXICO 87545

An Affirmative Action/Equal Opportunity Employer

UNITED STATES
ENERGY RESEARCH AND DEVELOPMENT ADMINISTRATION
CONTRACT W-7405-ENG. 36

Printed in the United States of America. Available from
National Technical Information Service
U.S. Department of Commerce
5285 Port Royal Road
Springfield, VA 22161
Price: Printed Copy $3.50 Microfiche $2.25

# NEUTRON BACKGROUND SPECTRA AND SIGNAL-TO-BACKGROUND RATIO FOR NEUTRON PRODUCTION BETWEEN 10 AND 14 MeV BY THE REACTIONS $^{3}H(p,n)^{3}He$, $^{1}H(t,n)^{3}He$, AND $^{2}H(d,n)^{3}He$

by

Manfred Drosg, George F. Auchampaugh, and Flavio Gurule



ABSTRACT

The monochromaticity of a "single line" neutron source is of utmost importance whenever secondary neutron yields over a wide energy range must be measured. Among the neutron sources considered, $^{3}H(p,n)^{3}He$ is best if a suitable beam stop is used; for example, $^{28}Si$ or $^{58}Ni$. Tantalum and gold give much larger backgrounds. Neutron emission spectra from the hydrogen gases and from various beam stops have been measured and are given in 1-MeV steps for primary neutron energies between 10 and 14 MeV.

## I. INTRODUCTION

For many neutron scattering experiments a pure monoenergetic neutron source is desirable. This is the case of neutron yield measurements pertinent to the design of controlled thermonuclear reaction (CTR) devices. The signal-to-background ratio of the neutron source is the limiting factor in determining the yield, especially for neutrons of lower energies. Therefore, the neutron source with the best signal-to-background ratio should be used to achieve reasonable uncertainties in the low-energy neutron yields. Data for incident neutrons below about 14 MeV are of special interest to the CTR program since this is the maximum average energy of neutrons from the $^{3}H(d,n)^{4}He$ reaction. Below 10 MeV it is not too difficult to have a clean source of monoenergetic neutrons. Therefore it is sufficient to investigate which source reaction gives the best signal-to-background ratio for energies between 10 and 14 MeV. We thus compared the neutron source reactions $^{3}H(p,n)^{3}He$, $^{1}H(t,n)^{3}He$, and $^{2}H(d,n)^{3}He$ in this energy interval. Since background neutrons originate not only from the interaction of the incident charged particles with the hydrogen gas inside the cell (i.e., breakup of the deuteron or triton), but also with the cell itself (i.e., primarily with the beam stop), and with the slits and collimators upstream of the cell, the effect of the beam stop or equivalently slit or collimator materials on the background was also investigated.

## II. EXPERIMENTAL

This experiment was performed at the Los Alamos Scientific Laboratory (LASL) Tandem Van de Graaff accelerator using a time-of-flight system with a liquid scintillator (NE-213) as a neutron detector. The experimental arrangement and the general experimental procedure have been described in Refs. 1 through 6. The arrangement used in this work differed in but two respects from the previous ones: the pulse height bias was set very low, at about 0.2 MeV corresponding proton energy, and the flight path was increased to about 3.7 meters. The latter change was necessary to reduce the multiple event probability to below 3% since the multiple event probability is increased strongly by lowering the bias. An error of the order of 3% due to the uncorrectable spectrum distortion by multiple events

was assumed acceptable as the aim of this investigation is the comparison among the source reactions only, for which data of 10% accuracy are sufficient.

The measurements were done with gas cells of 3-cm length. The gas pressure was about 1.7 atm for $T_2$ and $D_2$, and half as much for $H_2$. The pressure was recorded by means of a transducer with digital readout. The purity of the hydrogen gases was between 90 and 100%. This was determined by comparing the neutron yields with the known cross sections of the various reactions.[6,7] Such a comparison is independent of the knowledge of the neutron detector efficiency since it is done for only one neutron energy at a time.

Two types of cells were used. One had an entrance window of 5.3 mg/cm$^2$ molybdenum and a gold beam stop, while the other used isotopically pure $^{58}$Ni (enriched to 99.83%) for both the window (9.57 mg/cm$^2$) and the beam stop. The latter cell was used in connection with the $^3$H(p,n)$^3$He reaction only.

The neutron output from various beam stop materials was investigated by mounting discs of tantalum, $^{12}$C, and $^{28}$Si at the end of the beam tube. The $^{12}$C disc was enriched to 99.99%, the $^{28}$Si disc to 99.90%.

In order to get system-independent information on the signal-to-background ratio, it is necessary to separate the background from the gas from that of the cell (including background from the upstream beam line). Then the information derived can be used for many other experimental situations, e.g., for other gas pressures in the cell. So for each run with gas in the cell, an additional run was taken without gas, allowing background subtraction after normalizing to the same charge. This introduces some error due to the energy loss of the charged particles in the gas that does not occur in the empty cell. Therefore, low gas pressures were used, making this loss $\leq$ 30 keV for the p-T reaction, $\leq$ 40 keV for the t-H reaction, and $\leq$ 0.10 MeV for the d-D reaction. The rather large loss in the d-D case is insignificant since the background from the cell is small and practically negligible when compared with the background produced in the gas.

## III. RESULTS

Figures 1 through 5 summarize the results of this work for all five energies considered. The signal-to-background (S/N) ratio (number of monoenergetic neutrons over number of background neutrons of all sources) is given as a function of the areal density of the gas in the cell. Whereas the background produced in the beam stop is independent of the areal density of the gas, both the signal and the gas-associated background increases with gas pressure. Therefore, the signal-to-background ratio increases with pressure to a value given asymptotically by the ratio of the gas yield to gas background. This asymptotic value is indicated in the graphs by an arrow for the $^2$H(d,n)$^3$He reaction, and it is coincident with the upper frame line for the $^3$H(p,n)$^3$He reaction. This shows that the S/N ratio of the reaction $^3$H(p,n)$^3$He can be 3.3 times larger than that of $^2$H(d,n)$^3$He at 10 MeV and 5.5 times at 14 MeV. Therefore the $^3$H(p,n)$^3$He reaction is, intrinsically, at least an order of magnitude better than $^2$H(d,n)$^3$He in background-sensitive experiments, since the merit of a source reaction is very sensitive on the S/N ratio. The experimentally achieved ratios are near these maximum values, namely, 2.7 and 4.5, respectively (at 10 atm·cm).

These data include all neutrons above 0.3 MeV and are corrected for the detector efficiency and the dead time. Due to the low beam current (typically less than 20 nA), beam heating was negligible. The absolute error associated with these data is about 10%. If data for different reactions are compared at one energy, the uncertainty is even less since, in this case, some systematic errors cancel. On the other hand, one must keep in mind that these curves have been derived by measuring just one point (see graphs). Thus the exact answer for higher pressures will be somewhat lower because the energy loss in the gas will be increased, with a proportionate decrease in energy deposited in the beam stop and the mean energy of the particles passing through the entrance foil raised. This effect is not serious: at 14 MeV (the worst case) the S/N ratio of a practical cell with a $^{58}$Ni entrance foil and a $^{28}$Si beam stop would, at 10 atm·cm, deviate less than 10% from the value given by curve (a) in Fig. 5.

Figures 6 and 7 compare the neutron yields from the gas for the p-T and d-D source reaction at 10- and 14-MeV primary neutron energy. In this case the spectra are normalized to the same number of primary neutrons. It is evident that d-D is a poor choice because of the large background from the breakup of deuterons in the gas into neutrons and protons.

Figures 8 through 19 give the spectra of neutrons for the reaction p-T, d-D, and t-H generated from just the gas in the cell. The backgrounds from the beam stop and entrance foils have been removed from these data. The scale is given in mb/(sr·MeV) to allow the determination of neutron background per energy bin. It was derived from the known cross sections for the production of the primary neutrons (see Table I).

Although the energy loss in the gas, which was previously discussed, does not allow a precise background subtraction using the data from an empty cell, one can derive quite reliable zero degree cross sections for neutron production by breakup of the incident charged particle and/or the gas (see Table II).

Figures 20 through 30 give the neutron background of the cell with the gold beam stop and the molybdenum entrance foil for protons, deuterons, and tritons corresponding to primary neutron energies from 10 to 14 MeV. The scale is given in neutrons/(sr·MeV·nC).

Figures 31 through 35 give the neutron background for protons hitting a cell with entrance foil and beam stop made of $^{58}$Ni. This cell had been in use for more than five years, e.g., for the measurements reported in Ref. 2.

Since the good S/N ratio of the p-T reaction depends strongly on the cell used to contain the $T_2$ gas, a search was made to look for a suitable beam stop material with minimum neutron output when bombarded with protons. $^{28}$Si and $^{12}$C were considered since they have higher Q values for the p,n reaction than $^{58}$Ni. Tantalum was also investigated to compare with a gold beam stop.

Tantalum proved to be somewhat inferior to gold and was not considered further. Although $^{12}$C with its Q value of -18.13 MeV should give no neutron background at all, the background from the carbon beam stop was actually greater than that from the $^{58}$Ni beam stop which has a lower Q = -9.35 MeV. This is due to impurities of $^{13}$C with Q = -3.03 MeV generated by the decay of $^{13}$N which had built up during previous runs through the reaction $^{12}C(p,\gamma)^{13}N$. Therefore, $^{12}$C appears not to be a good choice as beam stop material.

The best results were obtained with a beam stop made of metallic $^{28}$Si, as can be seen in Fig. 36. This figure compares the neutron output for protons of 14.9 MeV incident on $^{12}$C, $^{28}$Si, and $^{58}$Ni. The advantage of using $^{28}$Si is obvious.

Figures 37 through 39 give the neutron output for protons of energies 10.9 to 14.9 MeV incident on the $^{28}$Si beam stop.

The absolute error in the spectra shown is estimated to be ± 10%, except for the spectra of $^{28}$Si. These spectra contain some background from upstream, from beam hitting slits, and from the defining aperture that could not be subtracted. Thus the spectra shown in Figs. 37 through 39 represent an upper limit only. This shows that for low

TABLE I

REFERENCE CROSS SECTIONS (0° LAB VALUES) USED IN THIS INVESTIGATION

| Neutron Energy (MeV) | $^{3}H(p,n)^{3}He$ (mb/sr) | $^{2}H(d,n)^{3}He$ (mb/sr) | $^{1}H(t,n)^{3}He$ (mb/sr) |
|---|---|---|---|
| 10 | 28.4 | 86.8 | 487 |
| 11 | 31.3 | 92.2 | 459 |
| 12 | 34.4 | 96.1 | not used |
| 13 | 37.4 | 98.3 | not used |
| 14 | 40.2 | 99.2 | not used |

TABLE II

ZERO DEGREE CROSS SECTIONS IN THE LABORATORY SYSTEM FOR BREAK-UP NEUTRONS FROM INTERACTION WITH THE GAS

(Scale error is ± 15%)

| Primary Neutron Energy (MeV) | $E_p$ (MeV) | p on $T_2$ $\frac{\sigma}{\text{(mb/sr)}}$ | $E_d$ (MeV) | d on $D_2$ $\frac{\sigma}{\text{(mb/sr)}}$ |
|---|---|---|---|---|
| 10 | 10.77 | 2.3 ± 0.1 | 6.83 | 22.6 ± 0.8 |
| 11 | 11.77 | 3.5 ± 0.2 | 7.87 | 47 ± 1.5 |
| 12 | 12.77 | 5.6 ± 0.4 | 8.92 | 80 ± 2.5 |
| 13 | 13.77 | 8.2 ± 0.4 | 9.97 | 120 ± 4 |
| 14 | 14.77 | 12.0 ± 0.9 | 11.03 | 162 ± 8 |

background systems not only the beam stop material but also the material of the aperture and of the slit coating should be chosen for minimum neutron background, unless the beam is so stable and well defined that it does not hit either slits or aperture. Considering that the neutron yield from gold is about 30 times larger than that from $^{28}Si$, the necessity of these precautions is obvious. The absolute error includes uncertainties because of the spectrum distortion due to multiple events, uncertainties in the efficiency curve, and uncertainties in the reference cross sections. The uncertainties in the corrections (dead time, pressure adjustment, neutron attenuation, current integration, beam heating) are much smaller than 10% and therefore negligible. Below about 1 MeV the error in the spectra might be larger than 10%, since most uncertainties increase with decreasing energy (e.g., efficiency curve, multiple event losses, background subtraction).

The data show that an optimum practical gas cell for the $^{3}H(p,n)^{3}He$ reaction has a beam stop made of $^{28}Si$ and an entrance foil of $^{58}Ni$. The increase of background because of buildup of impurities in $^{28}Si$ by the proton beam was so small that it could not be measured, even after an irradiation with 1.3 μA of protons for nine hours. Since $^{58}Ni$ is cheaper and easier to use than $^{28}Si$, and since the cell background is quite low, it might be nearly as good a choice as $^{28}Si$, especially if background from upstream is substantial.

This investigation shows that $^{3}H(p,n)^{3}He$ is the best source reaction with regard to signal-to-background ratio throughout the energy range considered, if a suitable beam stop is used. There are two obvious situations where a different source may be more desirable: (a) for the same beam current and gas pressure, the $^{1}H(t,n)^{3}He$ source gives nearly a 20 times larger yield of primary neutrons and the $^{2}H(d,n)^{3}He$ reaction a 2.5 times larger yield; (b) the very high gamma flux of the (p,γ) reaction in some beam stop materials (e.g., $^{58}Ni$) may make it prohibitive to use the p-T reaction with this beam stop in gamma-sensitive experiments ($^{28}Si$ appears to be somewhat better in this respect, too). In these cases the t-H reaction with as high a pressure as possible is recommended if the triton can be accelerated to the energy required to yield the desired neutron energy.

REFERENCES


1. A. Niiler, M. Drosg, J. C. Hopkins, J. D. Seagrave, and E. C. Kerr, "n-$^{4}$He Elastic Scattering Near 20 MeV," Phys. Rev. C4, 36 (1971).

2. M. Drosg, D. K. McDaniels, J. C. Hopkins, J. D. Seagrave, R. H. Sherman, and E. C. Kerr, "Elastic Scattering of Neutrons from $^{3}$He Between 7.9 and 23.7 MeV," Phys. Rev. C9, 179 (1974).

3. D. K. McDaniels, M. Drosg, J. C. Hopkins, and J. D. Seagrave, "Angular Distributions and Absolute Cross Sections for the T(p,n)$^{3}$He Neutron Source Reaction," Phys. Rev. C6, 1593 (1972).

4. M. Drosg, "Accurate Measurement of the Counting Efficiency of a NE-213 Neutron Detector Between 2 and 26 MeV," Nucl. Instr. Meth. 105, 573 (1972).

5. D. K. McDaniels, I. Bergqvist, D. M. Drake, and J. T. Martin, "Beam Heating in Gas Targets," Nucl. Instr. Meth. 99, 77 (1972).

6. M. Drosg and D. M. Drake, "Absolute Differential Cross Sections for Neutron Production by the $^{2}H(d,n)^{3}He$ Reaction with $E_d$ from 6 to 17 MeV and by the $^{3}H(p,n)^{3}He$ Reaction with $E_p$ from 6 to 16 MeV," Los Alamos Scientific Laboratory report LA-5732-MS (1974).

7. Horst Liskien and Arno Paulsen, "Neutron Production Cross Sections and Energies for the Reactions T(p,n)$^{3}$He, D(d,n)$^{3}$He, and T(d,n)$^{4}$He," Nucl. Data Tables 11, 569 (1973).

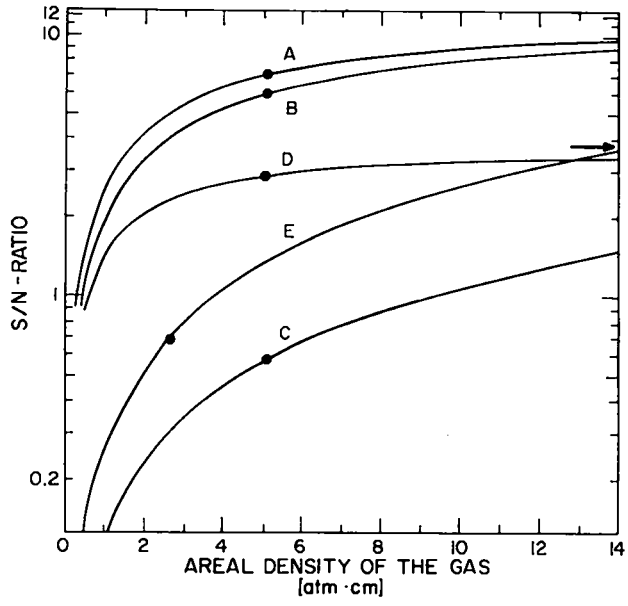


Fig. 1. Signal-to-background (S/N) ratio for 10-MeV primary neutrons.

(a) $^{3}H(p,n)^{3}He$ reaction using a $^{28}Si$ beam stop.
(b) $^{3}H(p,n)^{3}He$ reaction using a $^{58}Ni$ beam stop.
(c) $^{3}H(p,n)^{3}He$ reaction using a gold beam stop.
(d) $^{2}H(d,n)^{3}He$ reaction using a gold beam stop.
(e) $^{1}H(t,n)^{3}He$ reaction using a gold beam stop.

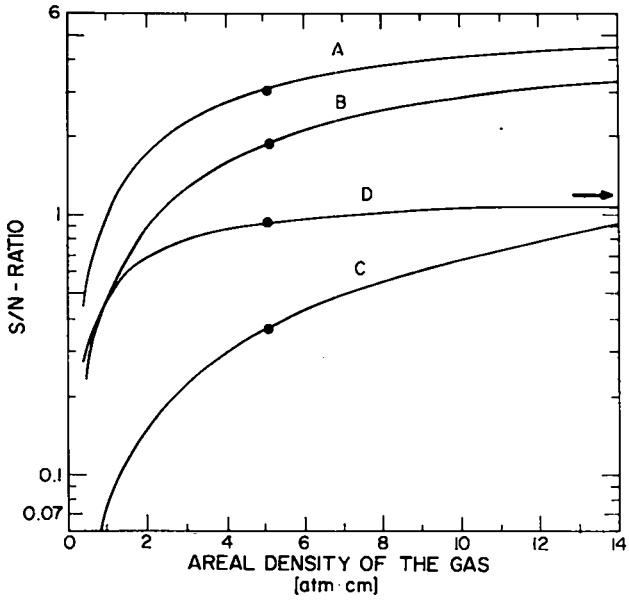


Fig. 3. Same as Fig. 1, except for 12-MeV primary neutrons.

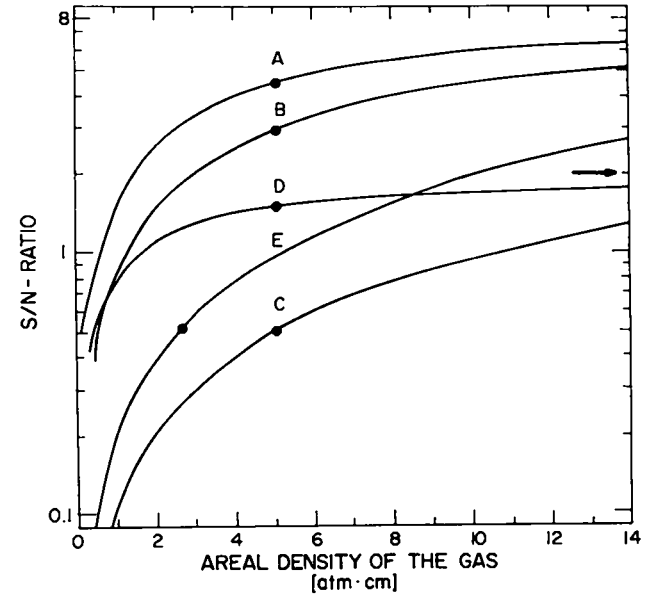


Fig. 2. Same as Fig. 1, except for 11-MeV primary neutrons.

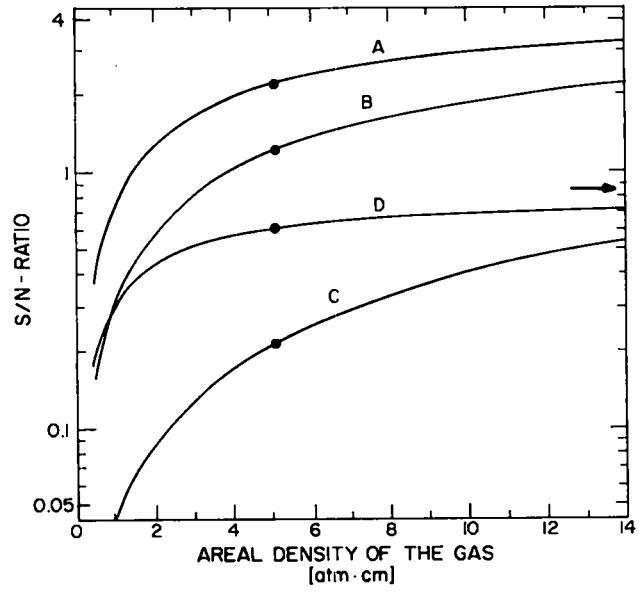


Fig. 4. Same as Fig. 1, except for 13-MeV primary neutrons.

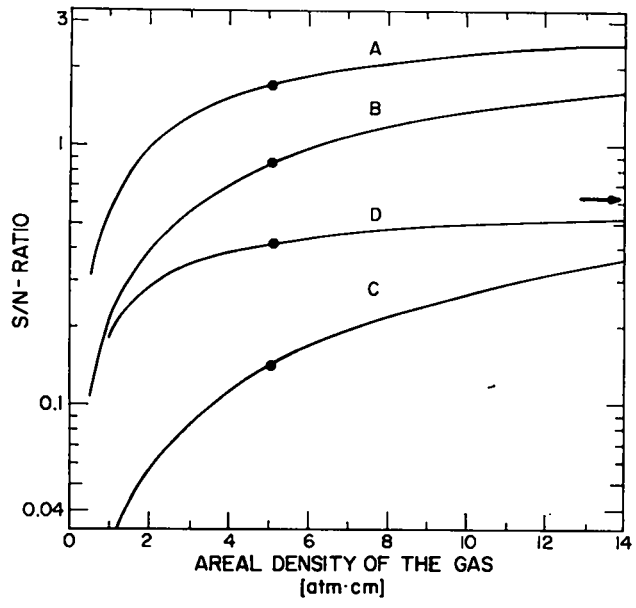


Fig. 5. Same as Fig. 1, except for 14-MeV primary neutrons.

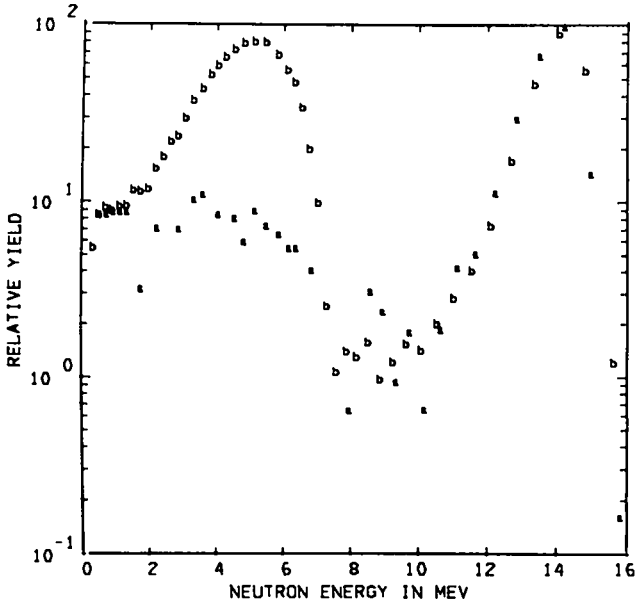


Fig. 7. Same as Fig. 6, except for 14-MeV primary neutron energy.

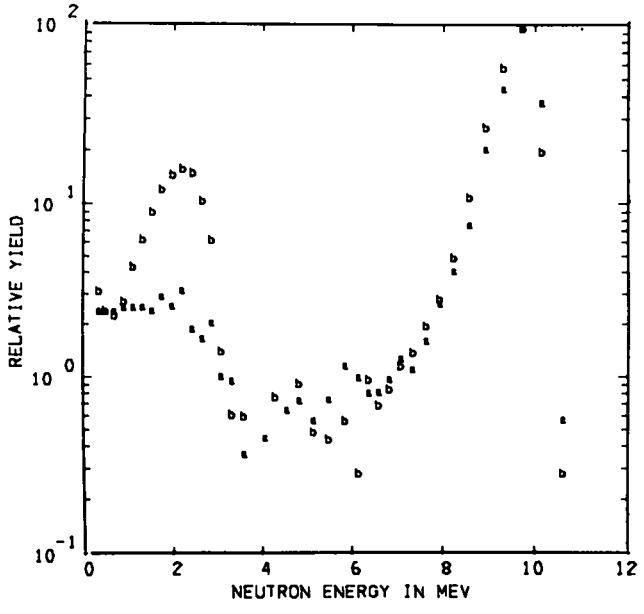


Fig. 6. Zero degree neutron spectra (gas yield only) from p on $T^{(a)}$ and d on $D^{(b)}$ normalized to the same primary neutron intensity for 10-MeV primary neutron energy.

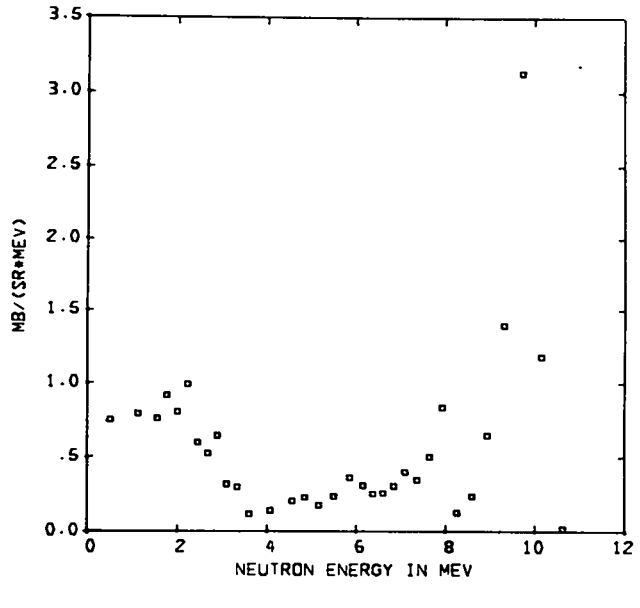


Fig. 8. Absolute double-differential neutron production cross sections at 0° for the reaction $^{3}H(p,n)^{3}He$ with primary neutrons at 10 MeV. The line itself is downscaled by a factor of 10.

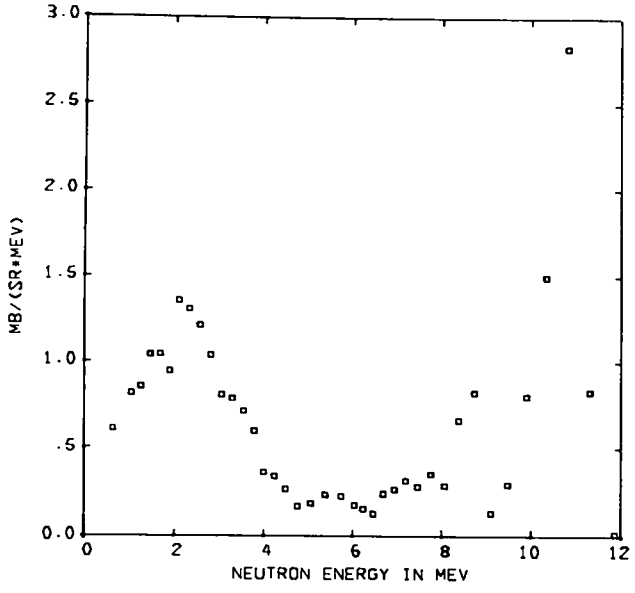


Fig. 9. Same as Fig. 8, except for 11-MeV primary neutrons.

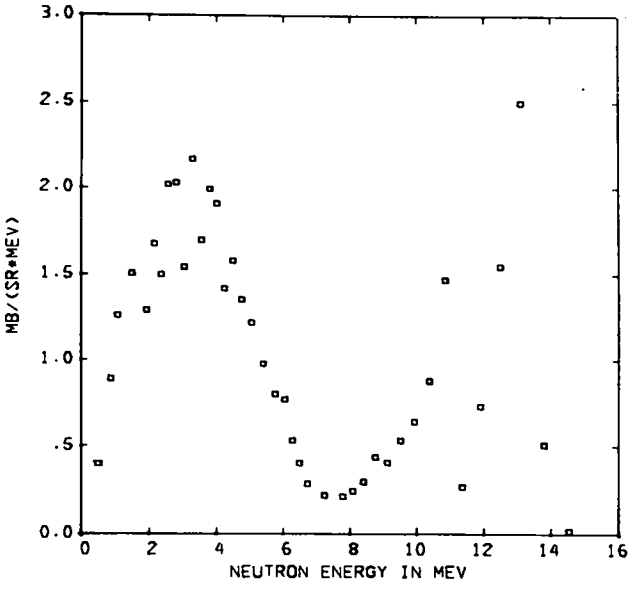


Fig. 11. Same as Fig. 8, except for 13-MeV primary neutrons.

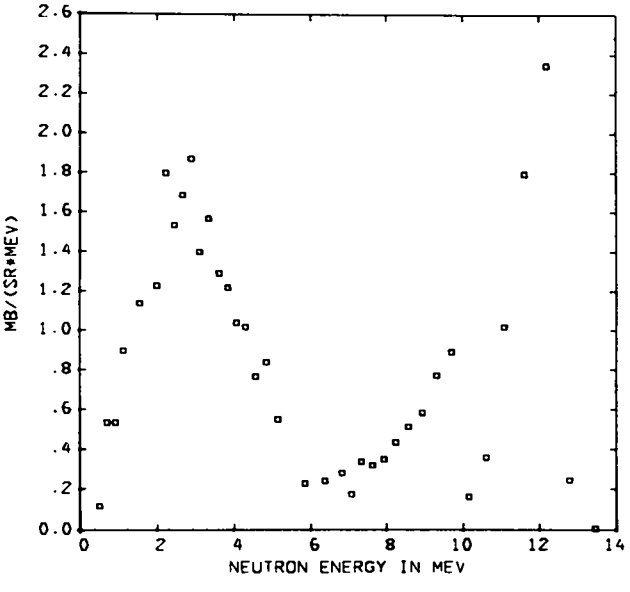


Fig. 10. Same as Fig. 8, except for 12-MeV primary neutrons.

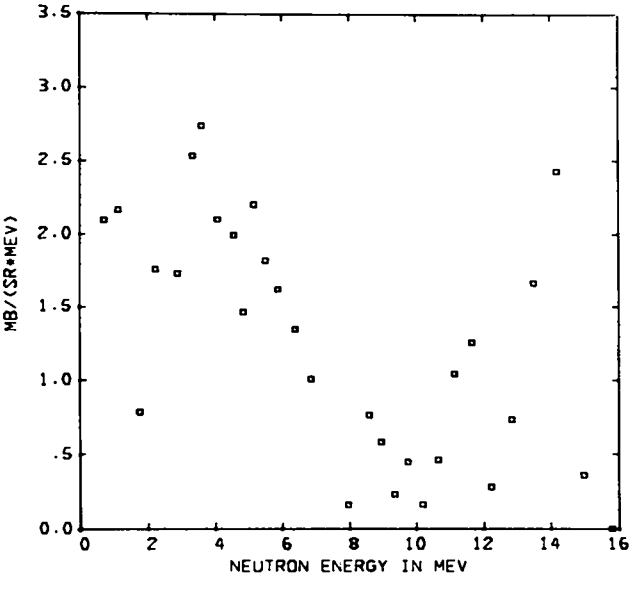


Fig. 12. Same as Fig. 8, except for 14-MeV primary neutrons.

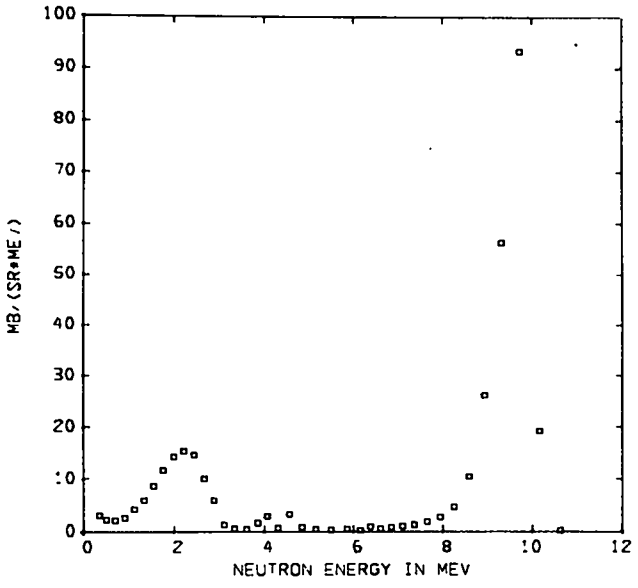


Fig. 13. Absolute double-differential neutron production cross sections at 0° for the reaction $^{2}H(d,n)^{3}He$ with primary neutrons at 10 MeV.

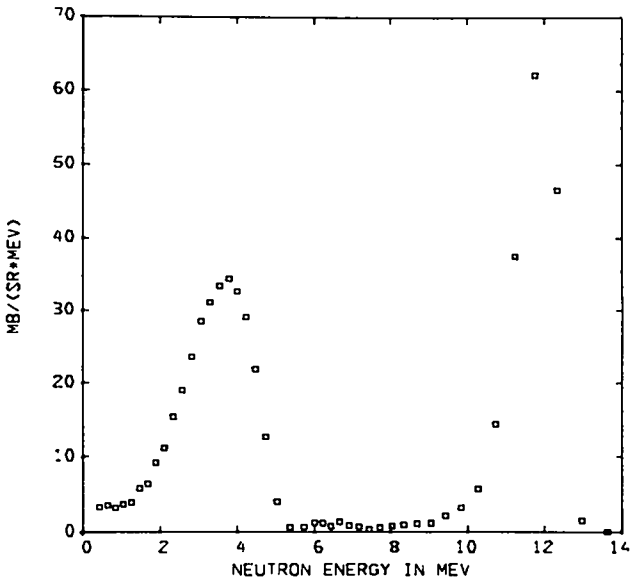


Fig. 15. Same as Fig. 13, except for 12-MeV primary neutrons.

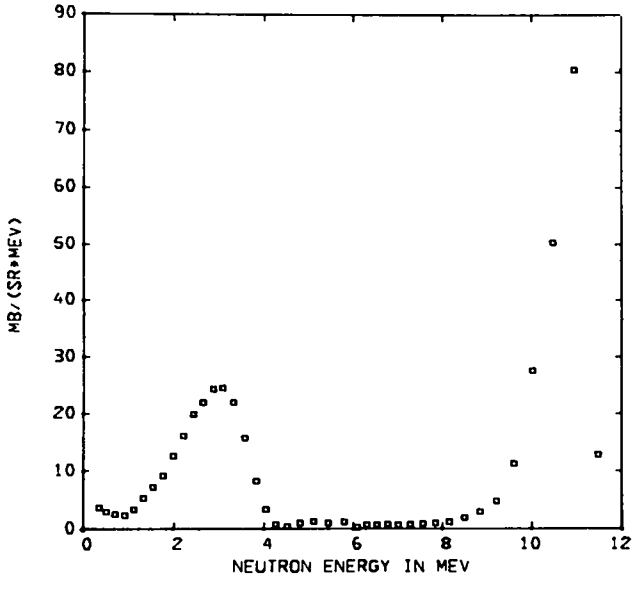


Fig. 14. Same as Fig. 13, except for 11-MeV primary neutrons.

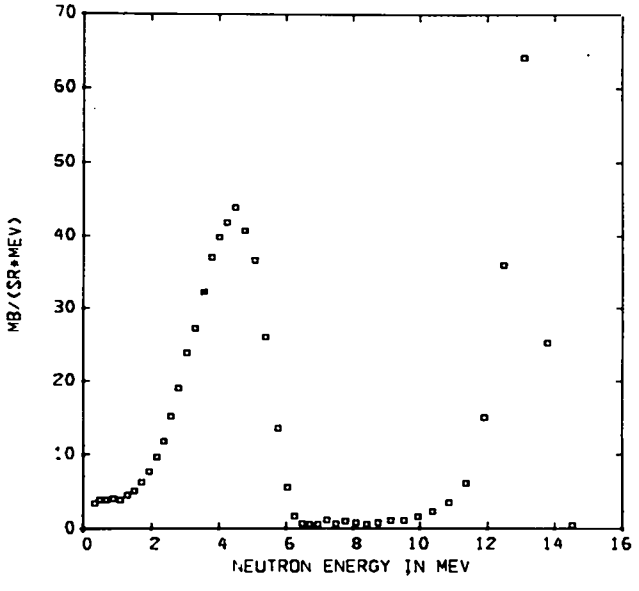


Fig. 16. Same as Fig. 13, except for 13-MeV primary neutrons.

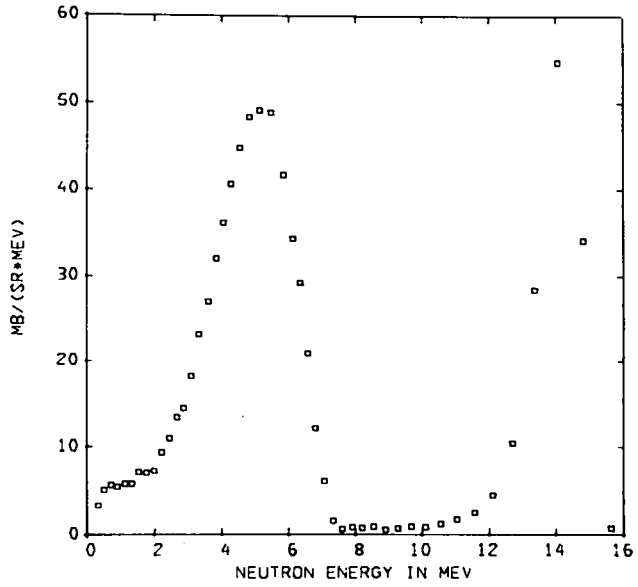


Fig. 17. Same as Fig. 13, except for 14-MeV primary neutrons.

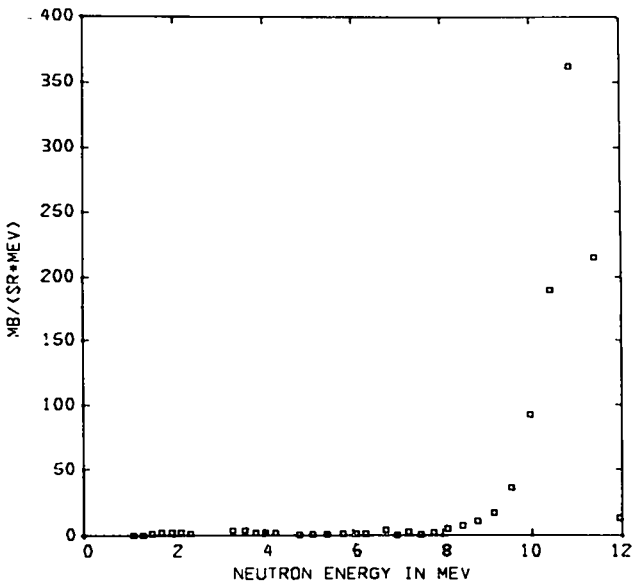


Fig. 19. Same as Fig. 18, except for 11-MeV primary neutrons.

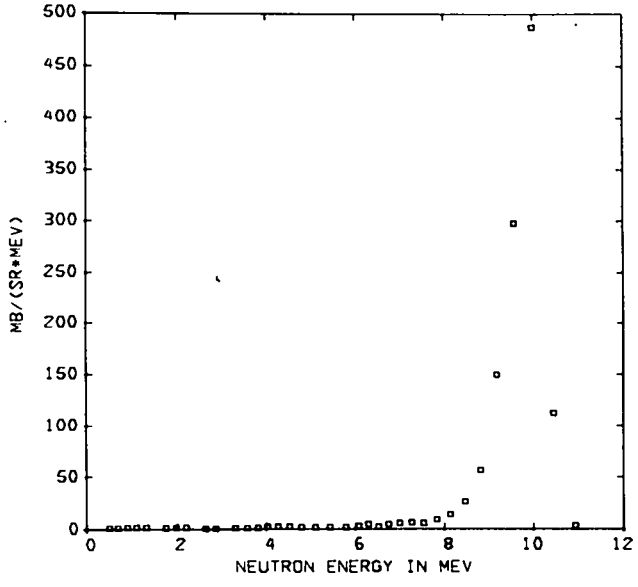


Fig. 18. Absolute double-differential neutron production cross sections at 0° for the reaction $^{1}H(t,n)^{3}He$ with primary neutrons at 10 MeV.

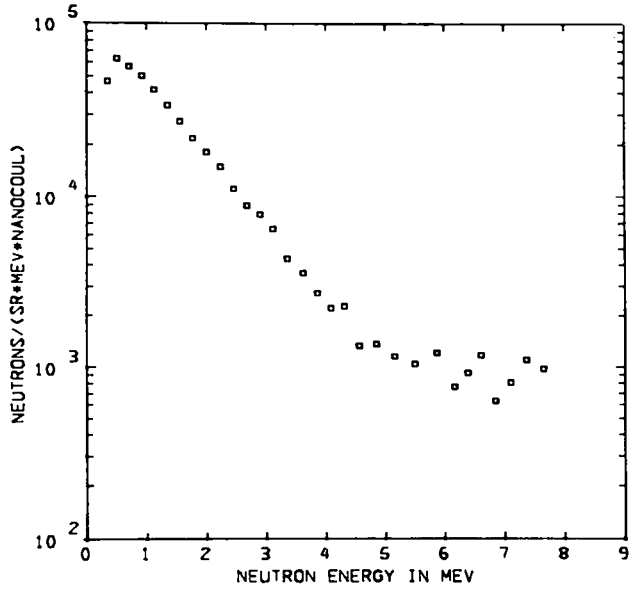


Fig. 20. Absolute numbers of neutrons per steradian·nanoCoulomb·MeV for 10.91-MeV protons hitting an empty cell with an entrance foil of 5.3 mg/cm$^2$ molybdenum and a gold beam stop.

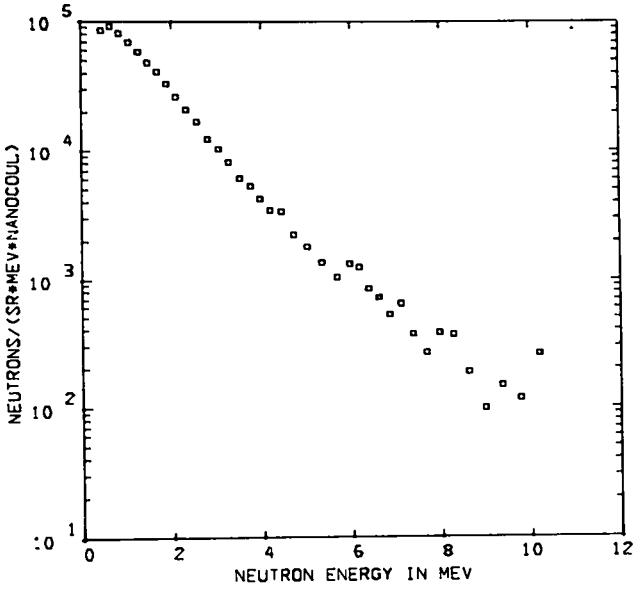


Fig. 21. Same as Fig. 20, except for 12.89-MeV protons.

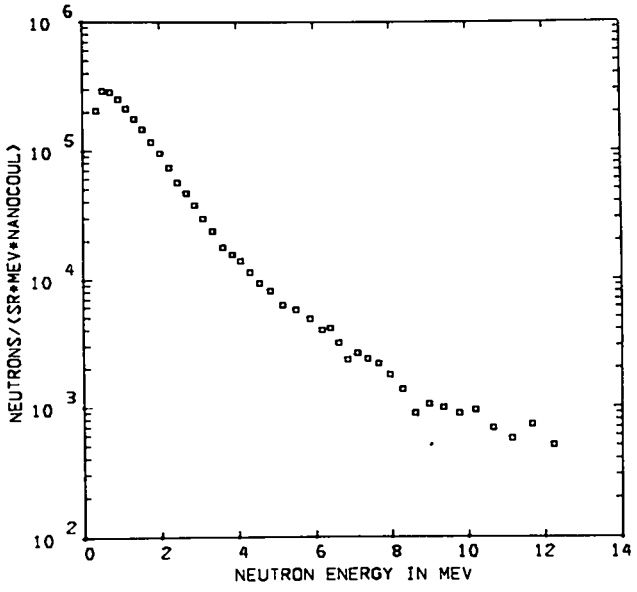


Fig. 23. Same as Fig. 20, except for 14.88-MeV protons.

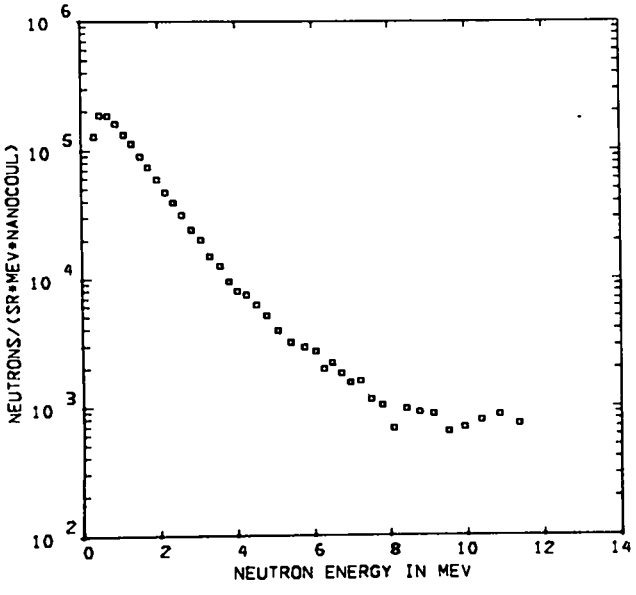


Fig. 22. Same as Fig. 20, except for 13.89-MeV protons.

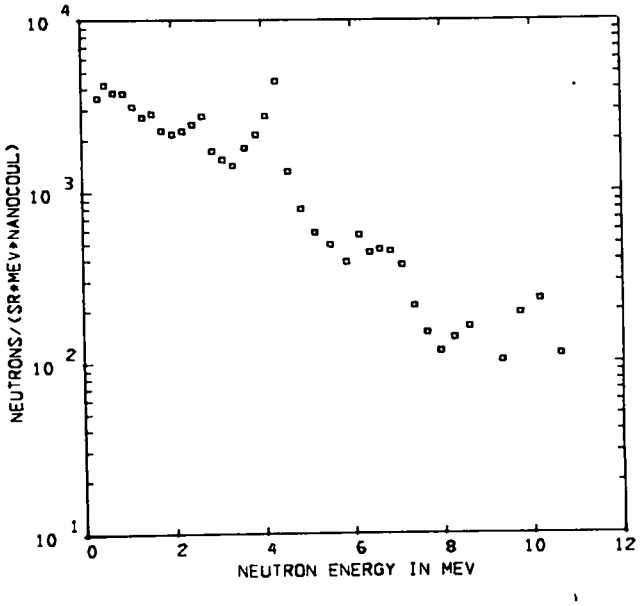


Fig. 24. Same as Fig. 20, except for 7.13-MeV deuterons.

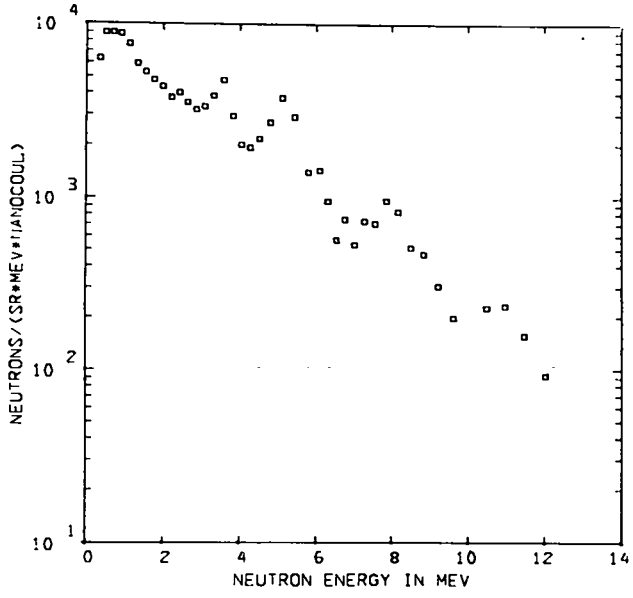


Fig. 25. Same as Fig. 20, except for 8.14-MeV deuterons.

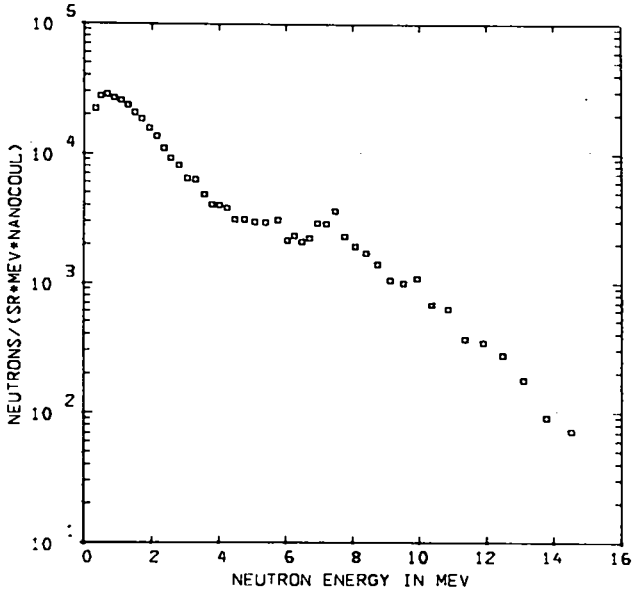


Fig. 27. Same as Fig. 20, except for 10.21-MeV deuterons.

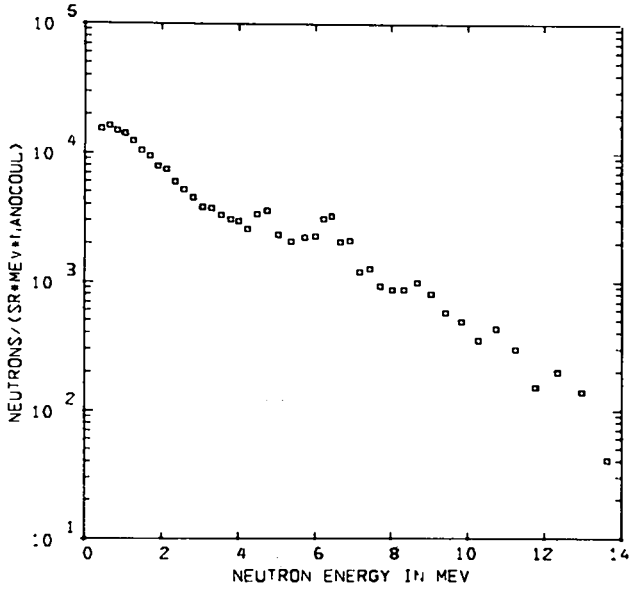


Fig. 26. Same as Fig. 20, except for 9.17-MeV deuterons.

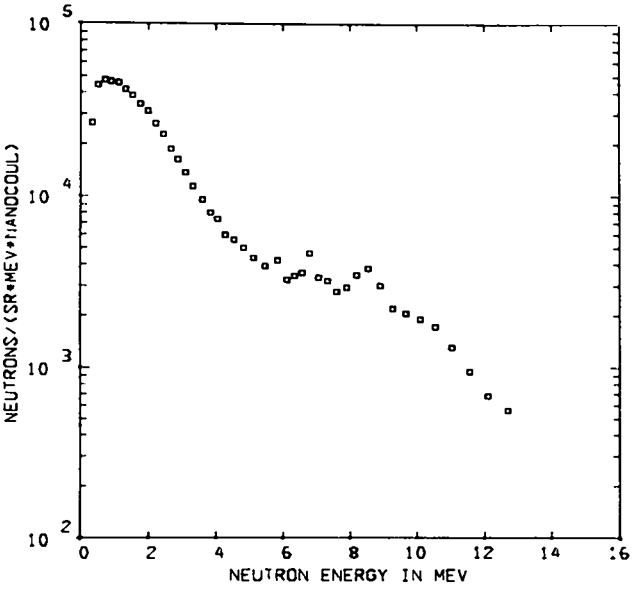


Fig. 28. Same as Fig. 20, except for 11.25-MeV deuterons.

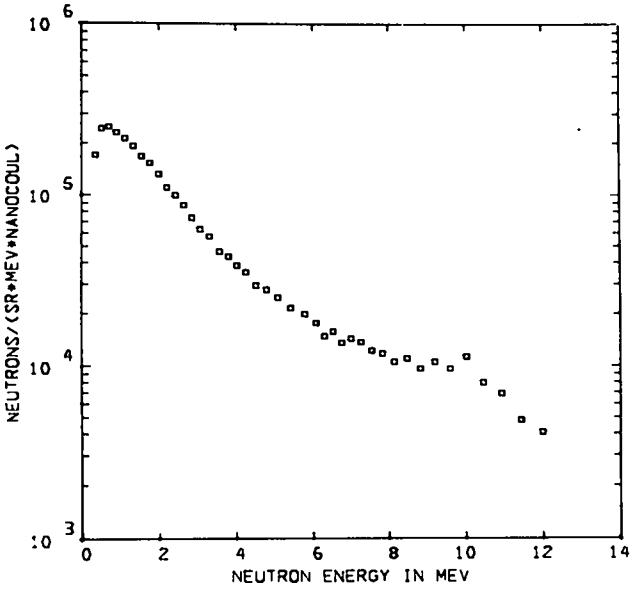


Fig. 29. Same as Fig. 20, except for 15.10-MeV tritons.

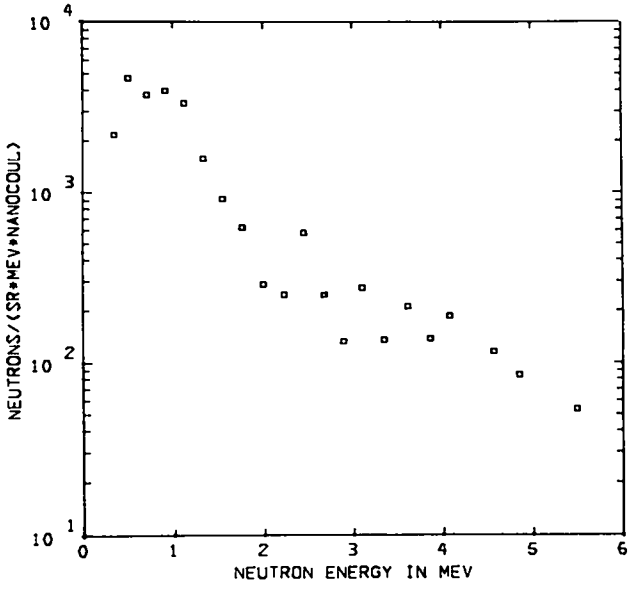


Fig. 31. Absolute numbers of neutrons per steradian·nanoCoulomb·MeV for 10.94-MeV protons hitting an empty cell with an entrance foil of 9.6 mg/cm$^2$ $^{58}$Ni and a beam stop made of $^{58}$Ni.

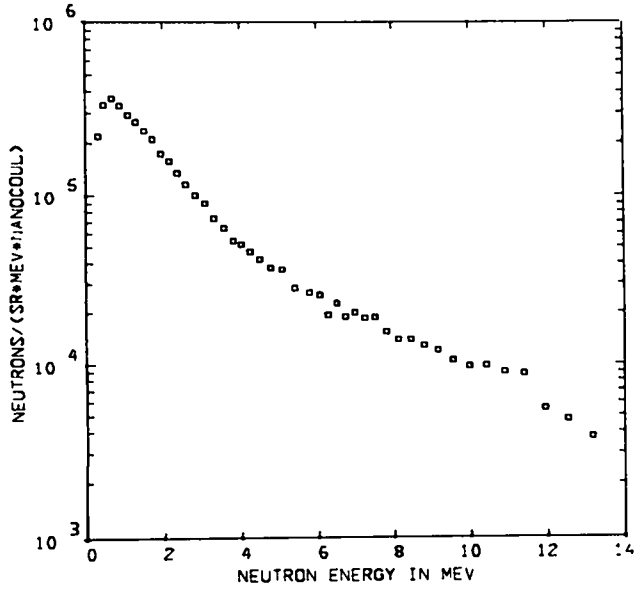


Fig. 30. Same as Fig. 20, except for 16.40-MeV tritons.

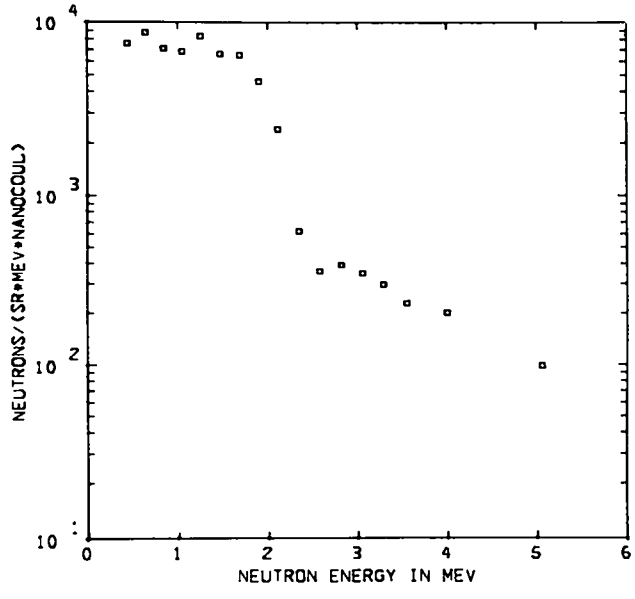


Fig. 32. Same as Fig. 31, except for 11.92-MeV protons.

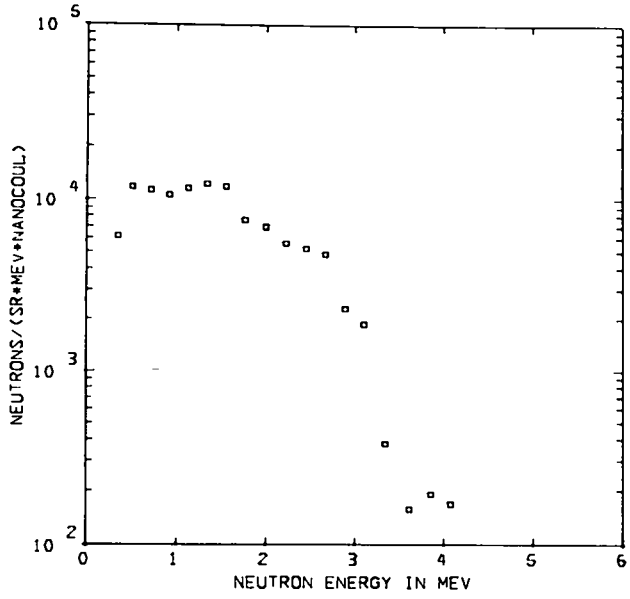


Fig. 33. Same as Fig. 31, except for 12.92-MeV protons.

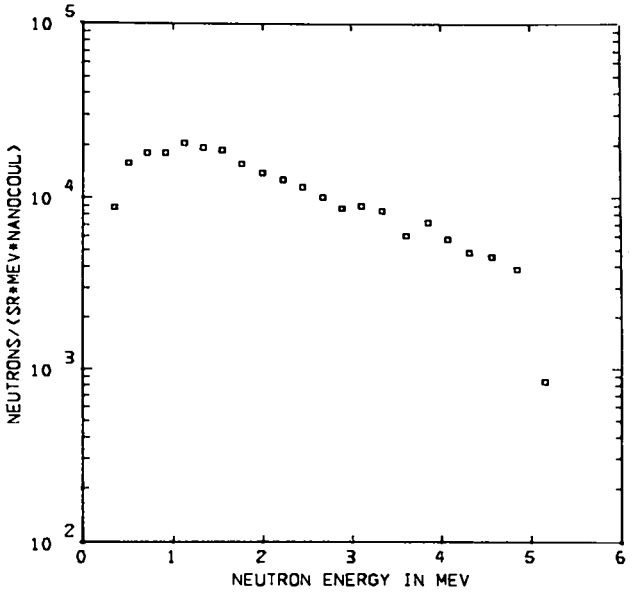


Fig. 35. Same as Fig. 31, except for 14.90-MeV protons.

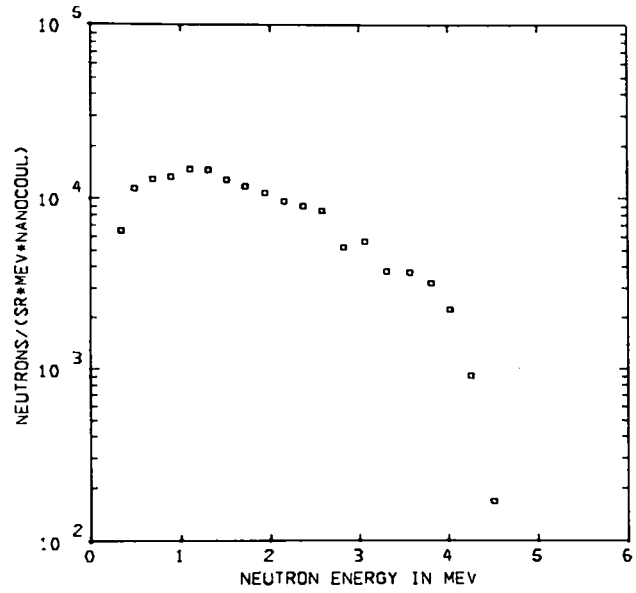


Fig. 34. Same as Fig. 31, except for 13.91-MeV protons.

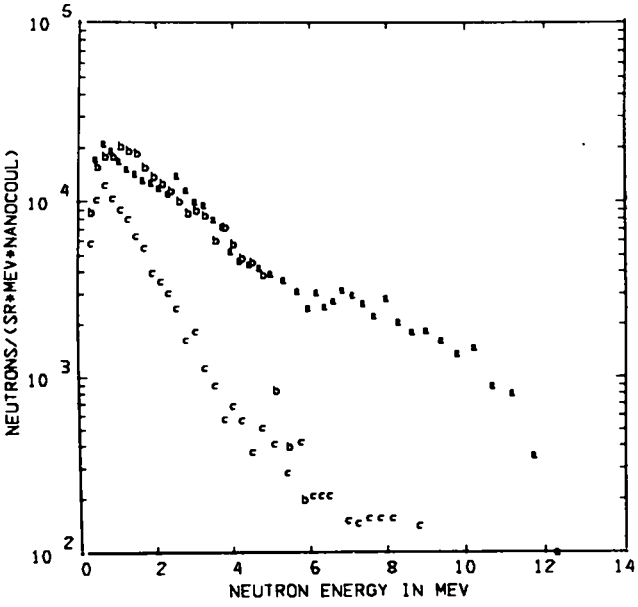


Fig. 36. Comparison of the neutron output of the best beam stop materials at 14.9-MeV incident proton energy.

a) $^{12}C$
b) $^{58}Ni$
c) $^{28}Si$

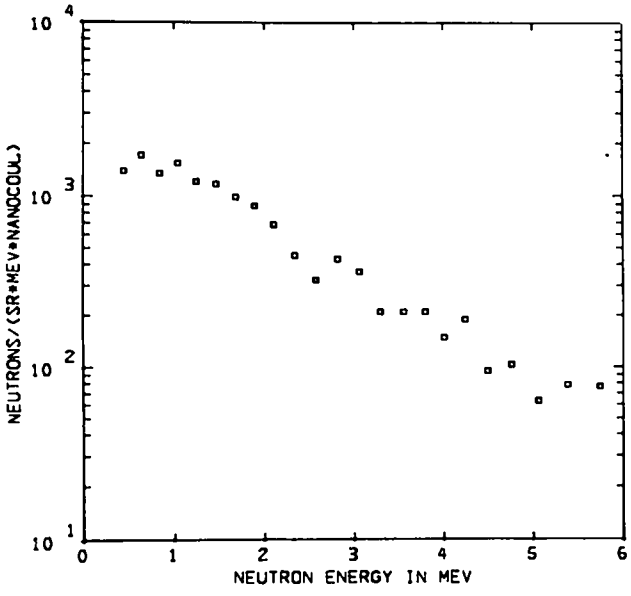


Fig. 37. Absolute number of neutrons per steradian steradian·nanoCoulomb·MeV for 10.94-MeV protons hitting a beam stop made of $^{28}Si$.

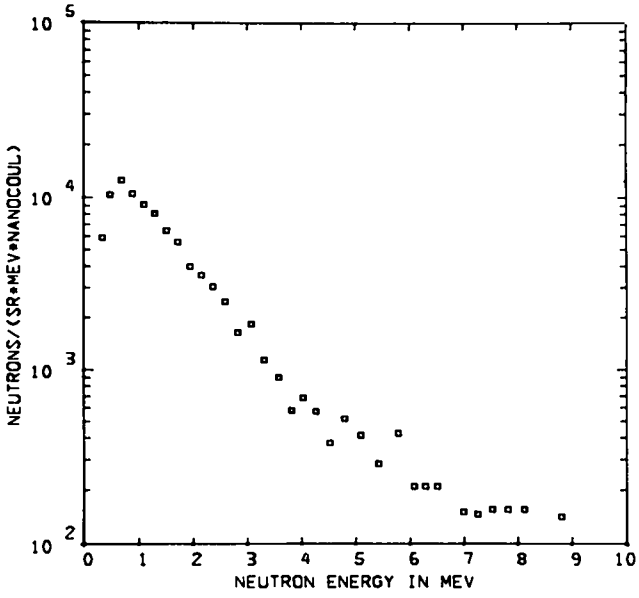


Fig. 39. Same as Fig. 37, except for 14.90-MeV protons.

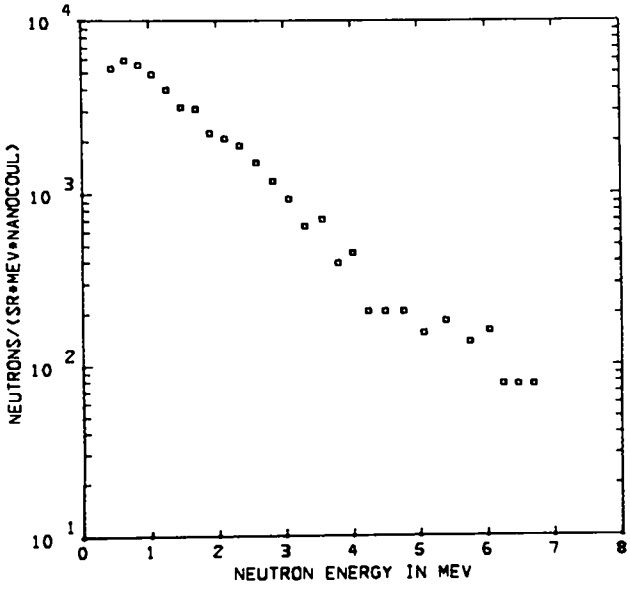


Fig. 38. Same as Fig. 37, except for 12.92-MeV protons.